

Journal of Materials Chemistry B

Accepted Manuscript



This is an *Accepted Manuscript*, which has been through the Royal Society of Chemistry peer review process and has been accepted for publication.

Accepted Manuscripts are published online shortly after acceptance, before technical editing, formatting and proof reading. Using this free service, authors can make their results available to the community, in citable form, before we publish the edited article. We will replace this *Accepted Manuscript* with the edited and formatted *Advance Article* as soon as it is available.

You can find more information about *Accepted Manuscripts* in the [Information for Authors](#).

Please note that technical editing may introduce minor changes to the text and/or graphics, which may alter content. The journal's standard [Terms & Conditions](#) and the [Ethical guidelines](#) still apply. In no event shall the Royal Society of Chemistry be held responsible for any errors or omissions in this *Accepted Manuscript* or any consequences arising from the use of any information it contains.

Pore Size Regulates Mesenchymal Stem Cell Response to Bioglass-Loaded Composite Scaffolds

Caroline A. B. Vissers, BS¹, Jenna N. Harvestine, BS¹, and J. Kent Leach, PhD^{1,2}

¹Department of Biomedical Engineering, University of California, Davis, Davis, CA USA

²Department of Orthopaedic Surgery, School of Medicine, University of California, Davis, Sacramento, CA, USA

Address for correspondence:

J. Kent Leach, Ph.D.
University of California, Davis
Department of Biomedical Engineering
451 Health Sciences Drive
Davis, CA 95616
Phone: (530) 754-9149
Fax: (530) 754-5739
Email: jkleach@ucdavis.edu

ABSTRACT

Composite scaffolds fabricated from synthetic polymers and bioceramics such as bioactive glasses are promising alternatives to autogenous bone graft for treatment of bone defects. Compared to other bioceramics, we previously demonstrated that bioactive glass (Bioglass 45S®, BG) further enhances the osteogenic program of bone-forming osteoblasts when incorporated into poly(lactide-co-glycolide) (PLG) macroporous scaffolds. However, cell response is dependent on parameters beyond scaffold composition including pore size and bioceramic availability to cells. We hypothesized that the osteogenic potential of human mesenchymal stem/stromal cells (MSCs) seeded on BG composite scaffolds was dependent upon pore diameter. Composite BG scaffolds were formed with three pore diameters – 125-300 μm , 300-500 μm , and 500-850 μm – by controlling porogen size. To determine the contribution of pore size on composite scaffold osteogenic potential, we characterized the biophysical properties, bioceramic distribution within the scaffold, and the osteogenic response of MSCs. All composite scaffolds were approximately 2-fold stiffer than the PLG control, and scaffolds with 500-850 μm pore diameters induced the greatest osteogenic response. The enhanced response of MSCs to scaffolds fabricated with large pores resulted from increased presentation of Bioglass along pore surfaces, enabling increased interaction between the cells and bioceramic. These data indicate that cellular behavior is dependent upon both pore size and material composition, confirming that the role of pore size should be considered in the development of new materials designed for bone repair.

Keywords: bioactive glass; pore size; scaffold; bone; tissue engineering

INTRODUCTION

Autogenous iliac crest bone graft remains the gold standard in treating large bone defects¹. Despite the successful clinical outcome, autografts are limited by morbidity at the tissue collection site, lack of sufficient bone graft volume, and potential for infection. The development of effective engineered scaffolds for bone tissue regeneration could benefit the millions of patients who suffer from bone defects due to trauma, disease, or congenital malformations².

The biophysical properties of scaffolds are dependent upon numerous parameters including porosity, pore diameter, interconnectivity, and degradation rate³. When considering properties of implantable scaffolds, high porosity and interconnectivity are desirable to facilitate vascular ingrowth⁴, while targeted degradation rate and mechanical strength depend on the rate of tissue ingrowth and implant environment, respectively⁵. The contribution of scaffold pore size in regulating tissue formation, however, remains an important topic of investigation. Small (<100 μm) pores result in greater surface area, allowing for increased cell adhesion, whereas larger pores facilitate cell migration, nutrient diffusion, and vascular invasion⁶. Pore diameter can directly affect cellular differentiation⁷, and *in vivo* models reveal that scaffolds possessing large pores yield more extensive bone ingrowth⁷. A pore size of 100 μm represents the functional lower limit for cell penetration and proper vascularization⁸, though the literature has not conveyed an upper boundary. As the porosity of native bone varies throughout the body, it is important to increase our understanding of how pore size within engineered scaffolds can instruct cell function.

The ideal bone scaffold would have appropriate mechanical strength for its implant site, support the growth and differentiation of bone-forming cells, and degrade *in situ* into non-harmful byproducts². Polymers boast desirable compliance and material degradation properties that can be anticipated *a-priori*, yet weak physical properties limit their application for bridging weight bearing bone. Implants formed entirely of bioceramics have significantly increased

mechanical properties, but are brittle and have slow degradation rates^{4, 9, 10}. Polymer/bioceramic composite scaffolds can be used to overcome these limitations and enhance the viability of scaffolds for treating large bone defects^{11, 12}. Our group previously reported the osteogenic and mechanical advantages conferred on poly(lactide-co-glycolide) (PLG) scaffolds by adding bioceramics such as hydroxyapatite, β -tricalcium phosphate, or bioactive glass (Bioglass, 45S®, BG)¹³. When keeping the relative mass composition of ceramic to polymer constant, BG-loaded composites had smaller pore diameters than corresponding scaffolds with other ceramics. Despite the heightened osteogenic potential of composite scaffolds¹⁴⁻¹⁶, particularly when incorporating Bioglass¹³, these constructs require further investigation to optimize their fabrication for balanced biological and mechanical properties.

We hypothesized that Bioglass composite scaffolds fabricated with small pore diameters would promote osteogenic differentiation of human mesenchymal stem/stromal cells (MSCs) through increased contact with the bioceramic compared to scaffolds with larger pore diameters. Conversely, scaffolds formed with larger pore diameters would facilitate increased cellular migration and growth at a cost of lower osteogenic response. To test our hypothesis, BG composite scaffolds were formed with three distinct pore diameters, modulated by the size of the porogen used in fabrication. We evaluated the biophysical properties and bioceramic distribution within the scaffolds, as well as the osteogenic response of human MSCs.

MATERIALS AND METHODS

Scaffold preparation

Scaffolds were fabricated using a gas foaming/particulate leaching method as previously described^{16, 17}. Poly(lactide-co-glycolide) (PLG) microspheres were formed from PLG pellets (85:15 DLG 7E; Lakeshore Biomaterials, Birmingham, AL) using a double-emulsion process and lyophilized to form a free-flowing powder. Microspheres (7.1 mg) were mixed with 17.8 mg

45S5 Bioglass® particulate (BG, 90–170 μm particle size, Novabone, Alachua, FL) and 135.1 mg NaCl particles (125-300 μm , 300-500 μm , or 500-850 μm in diameter), creating a 2.5:1:19 mass ratio of ceramic:polymer:salt¹⁶. Porogen diameter ranges were achieved by grinding the NaCl crystals, followed by separation using sieves corresponding to the desired crystal diameter. Control PLG scaffolds were synthesized without Bioglass using 250-425 μm diameter NaCl crystals, as this is the normal range currently employed by our group and others^{13, 18-20}. The powdered mixture of polymer, BG, and NaCl was then compressed using a Carver Press (Carver, Inc., Wabash, IN) and stainless steel die for one minute at 10 MPa to form solid disks of 8.5 mm diameter and 1.5 mm thickness. Polymer fusion was accomplished by placing the scaffolds in a custom-made high pressure (5.5 MPa) CO₂ gas chamber for 16 hours, followed by rapid release to atmospheric pressure. Scaffolds were then placed in DI water for 24 hours to remove the salt particles.

Prior to cell seeding, all scaffolds were submerged in a vacuum chamber with 0.1M NaOH for 2 minutes to functionalize the polymer surface and then rinsed with DI water. Scaffolds were sterilized in 70% ethanol for 30 minutes followed by two 15-minute rinses in sterile PBS, and one final 15-minute rinse in culture medium.

Scaffold characterization

Samples were gold coated using a sputter coater (Desk II; Denton Vacuum, Moorestown, NJ) for imaging with a scanning electron microscope (Hitachi S3500-N, Hitachi Science Systems Ltd, Tokyo, Japan) at 5 kV. This enabled the visualization of gross morphology and pore architecture within the scaffolds. The pore diameter of each scaffold was measured in ImageJ (National Institute of Health, Bethesda MD).

Porosity (void volume) was calculated by measuring the total volume of the scaffold before and after confined compression of the pores at 10 MPa for 30 seconds using a Carver

Press. The compression was performed within a stainless steel die in order to allow for changes in scaffold thickness while maintaining a constant diameter. Scaffold dimensions were measured with calipers before and after compression.

Permeation velocity of fluid flow through the scaffolds was measured as an indicator of pore connectivity. Briefly, silicon molds were cut with an 8 mm biopsy punch and press fit to the bottom of a syringe. Scaffolds were placed in the mold to ensure all collected media from the syringe traveled solely through the scaffold. The syringe was filled with osteogenic media, and the volume that passed through the scaffold at a given time was recorded. Permeation velocity was determined from perfusion volume, time, scaffold height, diameter, and media pressure drop using Darcy's Law.

The compressive moduli of composite scaffolds were determined using an Instron 5800 Series Testing System (Norwood, MA). Scaffolds were compressed with a constant deformation rate of 1 mm/min, and compressive modulus was calculated from the first 5% of strain¹⁶.

Trypan blue staining was used to grossly and qualitatively determine the distribution of BG throughout the scaffolds as described^{16, 18}. The stain binds to hydrophilic regions of the bioceramic, causing increased coloring in scaffolds with higher bioceramic availability. Scaffolds were immersed in 0.4% (w/v) Trypan blue solution (Alfa Aesar, Ward Hill, MA) for 15 seconds, then washed three times in DI water for 10 minutes, soaked in 100% ethanol for 1 minute, and washed again in DI water. These data were confirmed using energy dispersive spectroscopy (EDS) with analysis of the presence of carbon, oxygen, sodium, chlorine, calcium, and silicon (Hitachi S3500-N, Hitachi Science Systems Ltd, Tokyo, Japan).

Cell culture

Human bone marrow-derived mesenchymal stem/stromal cells (MSCs) (Lonza, Walkersville, MD) were purchased and used without further characterization. MSCs were

expanded in growth medium (GM) comprised of alpha medium (α -MEM; Invitrogen, Carlsbad, CA) supplemented with 10% fetal bovine serum (FBS; JR Scientific, Woodland, CA) and 1% penicillin-streptomycin (Mediatech, Manassas, VA) until use at passages 5-6. All cell culture was performed under standard conditions (37°C, 5% CO₂, 21% O₂).

Cells were statically seeded onto sterilized scaffolds at 7.5×10^5 cells/scaffold. Seeded scaffolds were incubated for 3 hours to allow for cell attachment, after which osteogenic media consisting of α -MEM plus standard osteogenic supplements (10 mM β -glycerophosphate, 50 μ g/mL ascorbate-2-phosphate, and 100 nM dexamethasone (all from Sigma Aldrich, St. Louis, MO)) was added. Seeded scaffolds were maintained on an XYZ shaker (Stovall, Greensboro, NC) at 25 rpm to facilitate media transport throughout the constructs, and media was changed every 3-4 days.

Sample collection

At designated time points, scaffolds were rinsed in PBS and then finely minced. The small cell-containing scaffold remnants were placed in 400 μ L of 1X passive lysis buffer (Promega, San Luis Obispo, CA) and vortexed for 5 seconds, and then centrifuged at 10,000 rpm for 5 minutes. The supernatant was stored at -20°C for biochemical assays.

To evaluate the level of cellular metabolic activity on seeded scaffolds, constructs were cultured in media containing a 10% (v/v) solution of AlamarBlue (Invitrogen, Frederick, MD) prior to scaffold collection. Scaffolds were incubated for one hour, conditioned media was collected, and fluorescence was measured at 570/585 nm on a microplate reader (Synergy HT, BioTek Instruments, Winooski, VT).

To assess cell infiltration into the scaffolds, constructs were collected and washed twice with PBS. Calcein AM (Invitrogen) staining solution was prepared per manufacturer's instructions to stain live cells. Samples were incubated in the staining solution on an XYZ

shaker at 25 rpm, 37°C, for one hour. After staining, samples were washed twice with PBS and fixed in 10% buffered formalin acetate (Fisher Scientific, Fair Lawn, NJ) for 6 hours. Samples were rinsed with 70% ethanol, then frozen at -80°C. Prior to sectioning, samples were placed on a vacuum filter, Tissue-Tek OCT Compound (Sakura Finetek, Torrance, CA) was perfused through the scaffold pores for 10 minutes on each side, and scaffolds were frozen. Tissue sections (5 µm) were cut on a Leica CM1850 Cryostat (Leica Microsystems, Bannockburn, IL) and mounted onto microscope slides for analysis. Sections were imaged using a Nikon Eclipse TE2000U microscope (Nikon Instruments, Melville, NY) and Andor Zyla digital camera (Oxford Instruments, Abingdon, Oxfordshire, United Kingdom).

Characterization of osteogenic differentiation

DNA was quantified using a Quanti-iT PicoGreen dsDNA Assay Kit (Invitrogen) per manufacturer's instructions. Phosphate salts were added to the passive lysis buffer at 400 mM concentration to liberate DNA from the mineral in the scaffolds^{21, 22}. Seeding efficiency was calculated by collecting samples after 4 hours of seeding and comparing DNA values to identical volume aliquots used to seed scaffolds.

Intracellular alkaline phosphatase activity (ALP) was quantified for all samples by incubating lysate with 50 mM *p*-nitrophenyl phosphate (PNPP) in assay buffer (100 mM glycine, 1 mM MgCl₂, pH = 10.5) at 37°C until a color change was observed. The absorbance was then measured at 405 nm using a plate reader (Biotek Synergy HT, Wisnooski, VT) and normalized to DNA as previously described^{16, 23}.

MSC-seeded scaffolds were cultured in osteogenic media for 21 days, fixed in formalin, and the distribution of bone formation within composite scaffolds was evaluated using high-resolution microcomputed tomography (microCT). Samples were placed in microcentrifuge tubes and allowed to warm to the CT scanner temperature (29°C) inside a custom plastic

holder. CT images were obtained on a MicroXCT-200 specimen CT scanner (Carl Zeiss X-ray Microscopy, Jena, Germany). The CT scanner has a variable x-ray source capable of a voltage range of 20-90kV with 1-8W of power. Samples were mounted on the scanner sample stage, which has submicron level of position adjustments. Source and detector distances were 35 and 15 mm, respectively; the manufacturer's LE4 custom filter was used for beam filtration; the voltage and power were set to 40 kV and 8 W, respectively; 1600 projections were acquired over 360-degrees with an exposure time of 3 seconds. Images were reconstructed on an isotropic voxel grid with 18.9377 microns per edge. Digital TIFF images were imported into Amira 5.6 (Visualization Sciences Group, FEI). For all specimens, 3D reconstructive images were generated to assess the spatial relationship of mineralized tissue.

STATISTICS

Statistical significance was determined using one-way ANOVA with Tukey's multiple comparison *post-hoc* tests. Probability values less than 0.05 were considered statistically significant. Unless otherwise indicated, groups not connected by the same symbol are statistically significant, and data are presented as means \pm standard error.

RESULTS

Porogen size mediates pore architecture and scaffold strength

Differences in pore architecture and morphological homogeneity were appreciable among the three scaffold pore conditions (**Fig. 1A**). Among scaffolds containing bioactive glass, scaffolds formed with porogens of 300-500 and 500-850 μm exhibited the most uniform honeycomb pattern. Scaffolds formed with porogen diameters of 125-300 μm appeared collapsed throughout the scaffold and did not visually exhibit evidence of interconnectivity. The resulting pore diameter of scaffolds was in good agreement with the average porogen size used

(**Fig. 1B**), yet higher variation was detected in scaffolds formed with the largest porogen. For simplicity, we denoted scaffold pore sizes as identical to the porogen diameter used during fabrication. Despite noticeable gross differences in pore size among the scaffolds, the porosity was similar for all three conditions (**Fig. 1C**), which was expected due to the same total volume of salt being added to each scaffold during synthesis. Scaffolds with larger pores enabled significantly faster fluid permeation compared to control scaffolds or composite scaffolds with the smallest pores, suggesting greater pore interconnectivity through the substrate (**Fig. 1D**).

Initial compressive moduli of acellular scaffolds were higher in all scaffolds containing bioceramic relative to scaffolds made entirely of PLG (**Fig. 2A**). After incubating in media for 21 days, the compressive moduli of the acellular composite scaffolds decreased to levels similar to PLG-only scaffolds (**Fig. 2B**).

Bioglass availability depends on pore diameter

Trypan blue staining revealed higher Bioglass surface availability in the 125-300 and 500-850 μm pore scaffolds. When compared to PLG controls lacking Bioglass, however, it became clear that staining of 125-300 μm pore scaffolds was falsely positive (**Fig. 3**). This is most likely due to decreased pore interconnectivity preventing the stain from washing out of the scaffold, as demonstrated in **Fig. 1D**. These results were confirmed using energy dispersive spectroscopy (EDS) to quantify the amount of Bioglass available on the surface of pore walls (**Fig. 4**). Composite scaffolds with 500-850 μm pores had a higher weight percentage of the four components of Bioglass: silicon, calcium, sodium, and phosphorus. The percentage of silicon and calcium on the surface, two critical elements that drive osteogenic response, increased significantly with increases in pore diameter (**Fig. 4B**). When acellular composite scaffolds were incubated over 21 days, we observed substantial reductions in the weight percentage of silicon

on the pore surface, suggesting its dissolution, while the mass percentage of calcium increased over time (**Fig. 4C**).

MSCs remain viable and migrate into composite scaffolds

We measured the capacity of MSCs seeded on composite scaffolds to remain viable and migrate into macroporous composite scaffolds. Metabolic activity at Day 1 (**Fig. 5A**) was in good agreement with perfusion velocity, suggestive that MSCs could migrate into the scaffolds more efficiently with larger pores. After 7 days in culture, we did not detect appreciable differences in AlamarBlue reduction. Representative fluorescence imaging of scaffold cross-sections revealed the distribution of cells at 1 and 7 days (**Fig. 5B**). We observed better penetration of MSCs in larger pore scaffolds at Day 1, yet most cells were evident on the periphery of all groups after 7 days, potentially due to nutrient limitations during culture.

Large pore composite scaffolds support cell proliferation and osteogenic differentiation

We evaluated the ability of each construct to support cell proliferation by quantifying DNA content on scaffolds at 7, 14, and 21 days. Seeding efficiency, analyzed from scaffolds 4 hours after seeding, was significantly higher in all composite scaffolds than the polymer control scaffold (**Fig. 6A**). Scaffolds with 500-850 μm pores contained more DNA, an indicator of higher cell numbers, than all other conditions at all time points (**Fig. 6B**). By Day 21, all three scaffolds exhibited lower DNA content relative to their starting values. MSCs seeded on large pore scaffolds (500-850 μm) exhibited significantly higher ALP activity at all time points, indicating enhanced osteogenic potential (**Fig. 6C**). Furthermore, normalized ALP activity was increasing at 21 days in large pore scaffolds, whereas it had plateaued in all other groups.

Mineral deposition is enhanced in large pore scaffolds

The quantity and spatial deposition of mineralized tissue within scaffolds was evaluated using microCT. Larger pores led to increased mineral deposition, as quantified by the percent mineral in each scaffold (**Fig. 7A**) and validated by CT images (**Fig. 7B**). Scaffolds fabricated with the largest pore diameters (500-850 μm) contained nearly three-times more mineral than scaffolds with intermediate pore diameters of 300-500 μm and more than 41-times more mineral than composite scaffolds with the smallest pore diameter. Two-dimensional sliced images of each scaffold were compiled to reveal a 3D compositional map, which exhibited greater mineral content and improved spatial distribution of mineral throughout the scaffold in larger pore scaffolds.

DISCUSSION

Biomaterial scaffolds designed for bone regeneration and repair require a balance of mechanical strength, handling potential for the clinicians, degradation rate, and the ability to stimulate the formation of new bone by cells that engage the substrate. Although many factors contribute to resolving these requirements, scaffold pore size is a critical parameter that affects these properties and has been inadequately investigated in scaffold design. In these studies, the incorporation of Bioglass in PLG scaffolds uniformly enhanced compressive moduli relative to PLG control scaffolds, regardless of pore size. Of the pore sizes measured in this study, scaffolds possessing pore diameters of 500-850 μm enabled increased Bioglass availability to cells, which enhanced cell proliferation and osteogenic response. Bioglass was not fully embedded within the polymer during manufacturing, facilitating increased interaction between BG and the seeded human MSCs that resulted in a more potent osteogenic response.

There is presently no consensus on the most effective range of pore sizes for scaffolds used in bone regeneration. Indeed, there is substantial variation in the porosity of native bone, and fabrication of biomaterial scaffolds with effective pore sizes must be performed with

knowledge of the intended implantation site. Previous studies assert that 300-400 μm is most effective for ectopic bone formation in ceramic scaffolds^{6, 24}. In contrast, others showed that polyester membranes with pore sizes under 200 μm promoted the most bone ingrowth in defects in the radii of rabbits²⁵. Additional *in vivo* results provided evidence that PLG-calcium phosphate composite scaffolds should have pore ranges of 500-1000 μm to maximize osteogenesis²⁶, with which our data most closely agree. These findings indicate that the pore size that maximizes bone formation is dependent not only on pore dimensions but also the composition of materials employed.

The incorporation of bioceramics into polymer scaffolds is a viable strategy to enhance the osteoconductive nature of implantable constructs for bone formation and repair. We selected Bioglass for inclusion in composite scaffolds based on our previous evidence of its superior osteogenic potential¹³. This study was further motivated by our unexpected observation of smaller pores in composite scaffolds loaded with Bioglass compared to other bioceramics. Other popular ceramics include hydroxyapatite (HA) and β -tricalcium phosphate (TCP), which have the advantage of maintaining higher porosity and compressive moduli over Bioglass when incorporated into composite scaffolds¹³. Unlike HA and TCP, Bioglass contains silica, which has been reported to significantly increase ALP activity and type I collagen production²⁷, two well-known indicators of osteogenic differentiation. Though cells have even more interactions with Bioglass in pure mineral scaffolds, the brittleness of these constructs makes them less attractive for use in bone regeneration. Moreover, HA and TCP resorb more slowly than Bioglass²⁸, representing an important consideration when determining how long the implant should remain in the defect. For these studies, we observed a marked reduction in compressive modulus in composite scaffolds after incubating acellular scaffolds in media for 21 days (**Fig. 2**). The reduction of composite scaffold stiffness to that of PLG control scaffolds suggests that the mineral dissolves over the 21-day timeframe. Therefore, mineral analyzed beyond this time point was attributed to new bone formation.

Our results confirmed greater bioceramic availability in scaffolds with larger pore diameters, indicating that the effect of large pores was due in part to the material employed. Though the same mass of Bioglass was incorporated into each scaffold, the physical presentation of the bioceramic into the pores was quantitatively different. Incorporation of Bioglass may be interfering with the capacity of PLG molecules to fuse to one another during the gas foaming manufacturing process. EDS allows for scanning of areas of a few μm^2 , which reveals the prevalence of the elements along a pore wall²⁹. These data suggest that more of the bioactive constituents in BG are available to cells. Moreover, composite scaffolds with larger pore diameters exhibited larger perfusion velocity, an indicator of pore interconnectivity, which likely enhances the presentation of BG dissolution components to neighboring cells. The increased availability of Bioglass and its components, particularly silica, has a strong impact on cellular response. We observed the most potent osteogenic response of MSCs on scaffolds with 500-850 μm pores, which had the greatest initial concentration of silicon and calcium on the pore surface and the greatest reduction in silicon mass on the pore surface after 21 days (**Fig. 4C**). Moreover, larger pore diameters would better enable the outward diffusion of Bioglass dissolution products that drive angiogenesis and resulting invasion of new blood vessels into the scaffold³⁰.

Our findings demonstrate the potential to tune the bioactive properties of composite scaffolds by modulating the availability of bioceramic as a function of pore size, thus providing an opportunity to further instruct cell function upon engagement with the substrate. These scaffolds can be used in defects that require careful attention to degradation rate while maintaining osteoconductivity. Porosity and degradation rate are important factors for bone ingrowth^{7, 31}, meaning the flexible and easily regulated degradation rate of poly(lactide-co-glycolide) coupled with the osteogenic properties of Bioglass create a promising platform for bone regeneration.

CONCLUSION

These data demonstrate that regulation of pore size provides an opportunity for optimizing composite scaffold-based technologies for bone regeneration. Individual materials should be tested with various pore sizes to elucidate changes in cell-scaffold interactions. Overall, pore size influences scaffold architecture and osteogenic potential, making it an important factor in scaffold design.

ACKNOWLEDGEMENTS

The project was supported by an award from the Orthopaedic Research and Education Foundation (#13-006) to JKL, the Arnold and Mabel Beckman Foundation to CABV, and a National Defense Science & Engineering Graduate Fellowship to JH. The authors gratefully acknowledge Doug Rowland, Ph.D., of the UC Davis Center for Molecular and Genomic Imaging for assistance with microCT analysis.

CONFLICT OF INTEREST DISCLOSURE

CABV, JH, and JKL declare that they have no conflict of interest.

REFERENCES

1. S. Zwingenberger, C. Nich, R. D. Valladares, Z. Yao, M. Stiehler and S. B. Goodman, *BioDrugs : clinical immunotherapeutics, biopharmaceuticals and gene therapy*, 2012, **26**, 245-256.
2. Q. Chen, J. A. Roether and A. R. Boccaccini, in *Topics in Tissue Engineering*, eds. E. N. Ashammakhi, R. L. Reis and E. Chiellini, 2008, vol. 4, ch. 6.
3. D. W. Hutmacher, J. T. Schantz, C. X. Lam, K. C. Tan and T. C. Lim, *Journal of tissue engineering and regenerative medicine*, 2007, **1**, 245-260.
4. Q. Z. Chen, I. D. Thompson and A. R. Boccaccini, *Biomaterials*, 2006, **27**, 2414-2425.
5. D. W. Hutmacher, *Biomaterials*, 2000, **21**, 2529-2543.
6. C. M. Murphy, M. G. Haugh and F. J. O'Brien, *Biomaterials*, 2010, **31**, 461-466.
7. V. Karageorgiou and D. Kaplan, *Biomaterials*, 2005, **26**, 5474-5491.
8. J. R. Jones, L. M. Ehrenfried and L. L. Hench, *Biomaterials*, 2006, **27**, 964-973.
9. P. V. Giannoudis, H. Dinopoulos and E. Tsiridis, *Injury*, 2005, **36 Suppl 3**, S20-27.
10. S. S. Kim, M. Sun Park, O. Jeon, C. Yong Choi and B. S. Kim, *Biomaterials*, 2006, **27**, 1399-1409.
11. K. Rezwani, Q. Z. Chen, J. J. Blaker and A. R. Boccaccini, *Biomaterials*, 2006, **27**, 3413-3431.
12. E. L. Hedberg, C. K. Shih, J. J. Lemoine, M. D. Timmer, M. A. Liebschner, J. A. Jansen and A. G. Mikos, *Biomaterials*, 2005, **26**, 3215-3225.
13. D. G. Morales-Hernandez, J. K. Leach, D. C. Genetos, D. M. Working and K. C. Murphy, *Journal of Functional Biomaterials*, 2012, **3**, 382-397.
14. T. Yoshii, J. E. Dumas, A. Okawa, D. M. Spengler and S. A. Guelcher, *Journal of biomedical materials research. Part B, Applied biomaterials*, 2012, **100**, 32-40.
15. S. Srouji, T. Kizhner and E. Livne, *Regenerative medicine*, 2006, **1**, 519-528.
16. J. He, D. C. Genetos and J. K. Leach, *Tissue engineering. Part A*, 2010, **16**, 127-137.
17. H. E. Davis, R. R. Rao, J. He and J. K. Leach, *Journal of biomedical materials research. Part A*, 2009, **90**, 1021-1031.
18. H. E. Davis, E. M. Case, S. L. Miller, D. C. Genetos and J. K. Leach, *Biotechnology and bioengineering*, 2011, **108**, 2727-2735.
19. L. Thorrez, J. Shansky, L. Wang, L. Fast, T. VandenDriessche, M. Chuah, D. Mooney and H. Vandenburgh, *Biomaterials*, 2008, **29**, 75-84.
20. L. D. Harris, B. S. Kim and D. J. Mooney, *Journal of biomedical materials research*, 1998, **42**, 396-402.
21. E. J. Arnsdorf, P. Tummala and C. R. Jacobs, *PLoS One*, 2009, **4**, e5388.
22. J. He, M. L. Decaris and J. K. Leach, *Tissue engineering. Part A*, 2012, **18**, 1520-1528.
23. B. Y. Binder, D. C. Genetos and J. K. Leach, *Tissue engineering. Part A*, 2014, **20**, 1156-1164.
24. E. Tsuruga, H. Takita, H. Itoh, Y. Wakisaka and Y. Kuboki, *Journal of biochemistry*, 1997, **121**, 317-324.
25. L. M. Pineda, M. Busing, R. P. Meinig and S. Gogolewski, *Journal of biomedical materials research*, 1996, **31**, 385-394.
26. L. G. Sicchieri, G. E. Crippa, P. T. de Oliveira, M. M. Beloti and A. L. Rosa, *Journal of tissue engineering and regenerative medicine*, 2012, **6**, 155-162.
27. E. J. Kim, S. Y. Bu, M. K. Sung and M. K. Choi, *Biological trace element research*, 2013, **152**, 105-112.
28. F. Barrere, C. A. van Blitterswijk and K. de Groot, *International journal of nanomedicine*, 2006, **1**, 317-332.

29. J. M. Karp, M. S. Shoichet and J. E. Davies, *Journal of biomedical materials research. Part A*, 2003, **64**, 388-396.
30. A. Leu and J. K. Leach, *Pharmaceutical research*, 2008, **25**, 1222-1229.
31. L. A. Solchaga, J. S. Temenoff, J. Gao, A. G. Mikos, A. I. Caplan and V. M. Goldberg, *Osteoarthritis and cartilage / OARS, Osteoarthritis Research Society*, 2005, **13**, 297-309.

FIGURE LEGENDS

Figure 1. (A) Scaffold pore morphology observed using scanning electron microscopy. Images were taken at 200X magnification; scale bar represents 400 μm . (B) Resultant pore diameter in scaffolds fabricated with increasing porogen diameter (n=4). (C) Scaffold porosity was determined by comparison of scaffold volume before and after crushing pores (n=5). (D) Permeation velocity of osteogenic media through scaffolds fabricated with increasing porogen diameter (n=4).

Figure 2. Influence of pore size on mechanical properties of acellular scaffolds. (A) Compressive moduli of composite scaffolds after fabrication; n=3 for 125-300 μm pore scaffolds, n=4 for 300-500 and 500-850 μm pore scaffolds, and n=22 for PLG scaffolds; ** $p < 0.01$ vs. all other groups. (B) Compressive moduli of acellular composite scaffolds when maintained in culture media for 21 days (n=3 for all groups).

Figure 3. Distribution of BG within composite scaffolds revealed by trypan blue staining. Representative images of trypan blue staining of composite scaffolds with 125-300 μm , 300-500 μm , and 500-850 μm pores and PLG scaffolds with identical pore sizes as control groups. Scale bar represents 1 cm.

Figure 4. Elemental distribution of BG in composite scaffolds. (A) EDS images demonstrating elemental distribution along pore walls of PLG control scaffolds with 250-425 μm pores and BG-PLG composite scaffolds with 125-300, 300-500, and 500-850 μm pores. (B) Table presenting the weight percentage of silicon and calcium on the pore surface in scaffolds with varying pore diameter (n=6; ^a $p < 0.0001$ vs. all other groups). (C) Table presenting the percent change in

weight percentage of silica and calcium on the pore surface in scaffolds with varying pore diameter after 21 days (n=6).

Figure 5. MSCs are viable and migrate into composite scaffolds. **(A)** Quantification of metabolic activity *via* AlamarBlue assay on composite scaffolds after 1 and 7 days in culture (n=4). **(B)** Representative fluorescent images of cell distribution in composite scaffolds at 1 and 7 days; scale bar represents 500 μm .

Figure 6. Characterization of MSC seeding and early osteogenic differentiation on composite scaffolds with increasing pore size. **(A)** Seeding efficiency of MSCs on composite and PLG control scaffolds, as measured by quantifying DNA amount, a measure of cell attachment. **(B)** DNA quantification on scaffolds at Day 0 (** $p < 0.01$ vs. all other groups within time point), Day 7 (** $p < 0.001$ vs. all other groups within time point); Day 14 ($p < 0.05$ vs. all other groups within time point); and Day 21 (** $p < 0.01$ vs. all other groups within time point). n=5 for all data. **(C)** Osteogenic differentiation of human MSCs on scaffolds as determined by ALP activity (n=6; $p < 0.05$ vs. 125-300 μm in time point; *** $p < 0.001$ vs. all other groups in time point).

Figure 7. Mineral distribution within composite scaffolds determined by microCT. **(A)** Percent mineral within total construct material, calculated using Amira software (n=3 for all groups). **(B)** Representative 2D image of scaffold cross-section. Mineral is outlined in red and PLG is outlined in dark green. Images are labeled with pore diameter (μm) of scaffold. **(C)** Representative 3D rendering performed by stacking 2D images of each cross-section from scaffolds with distinct pore diameters, revealing the total mineral in each scaffold. Mineral is shown in white and PLG in gray.

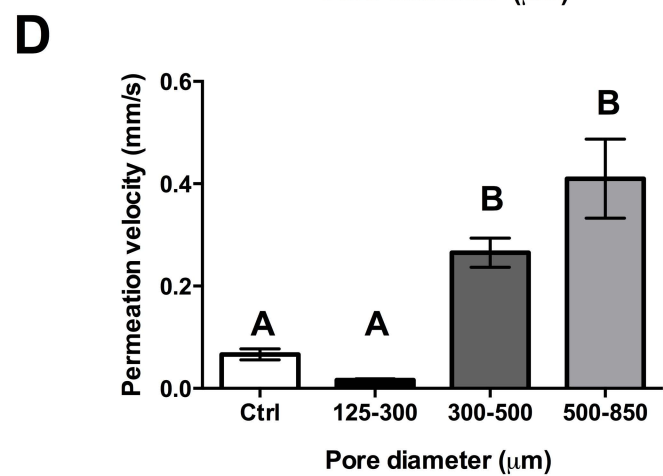
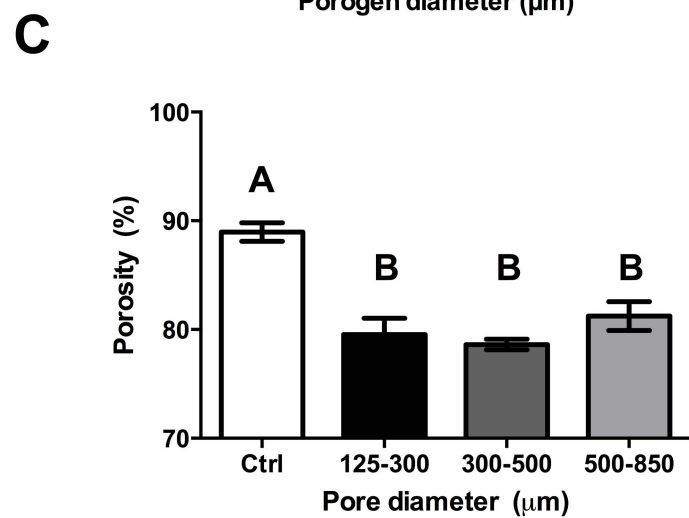
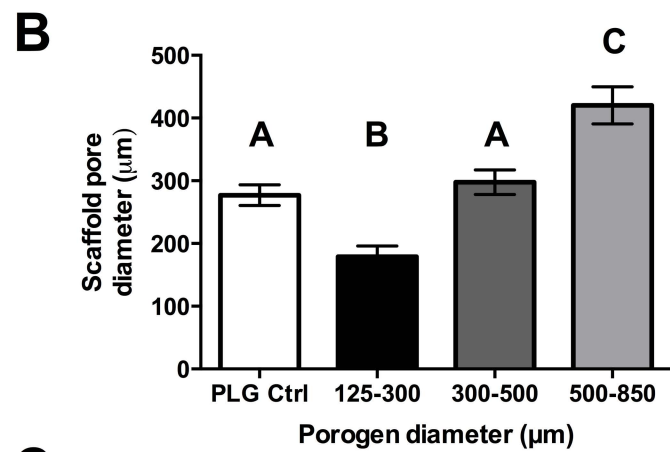
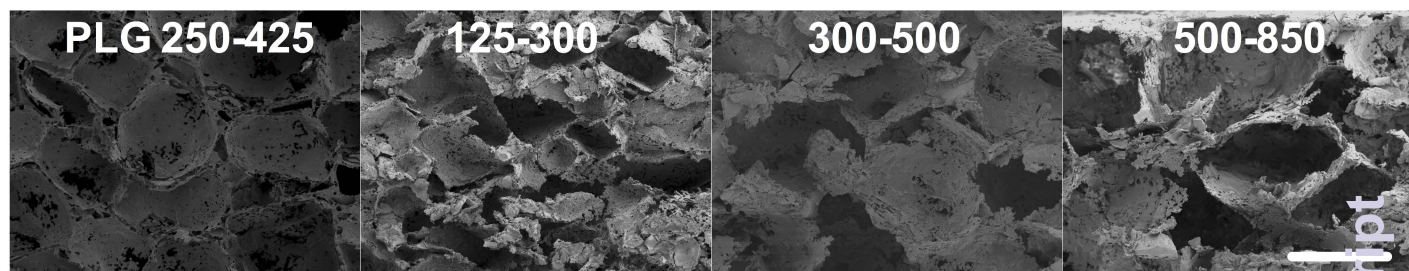
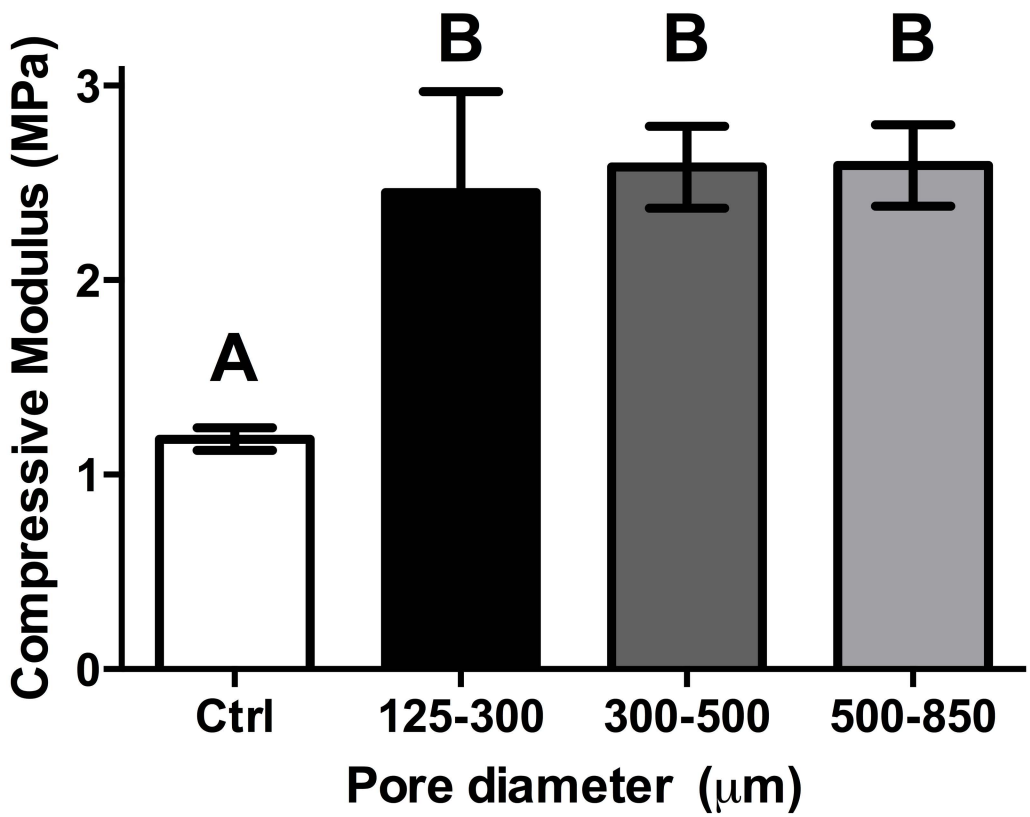


Figure 1



B

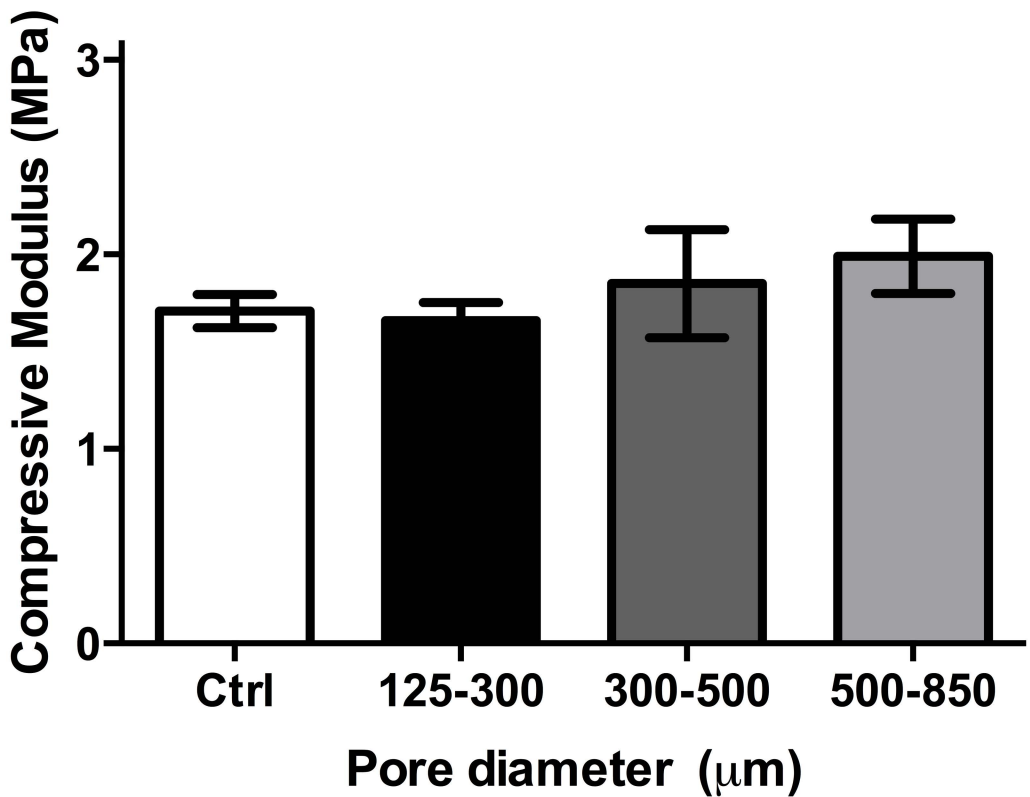
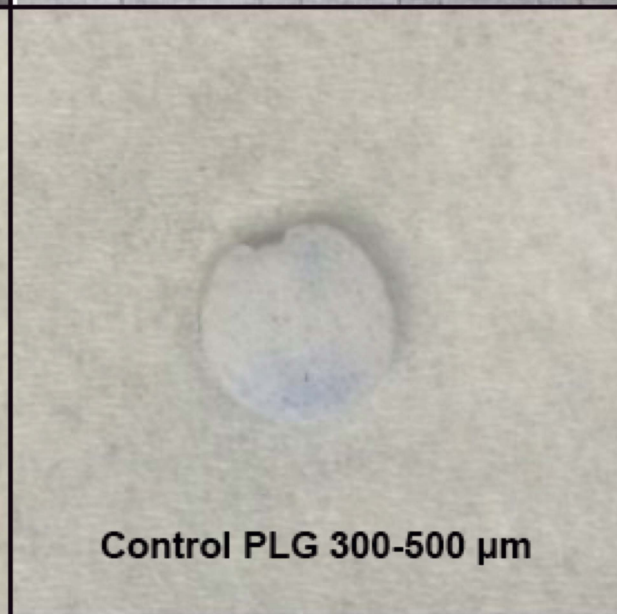
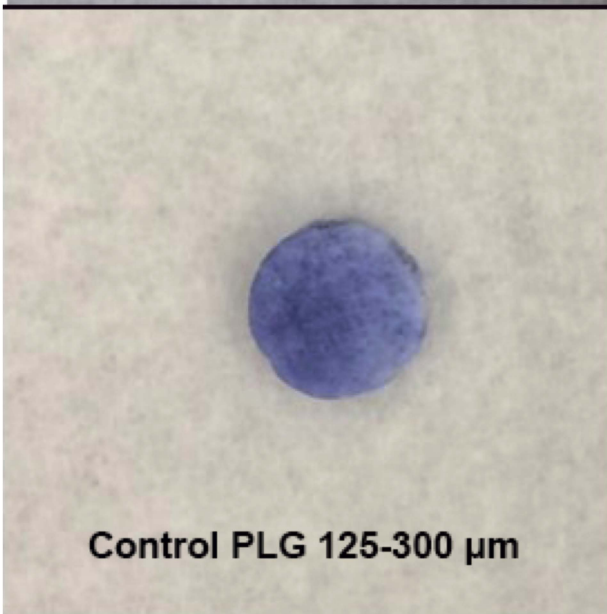
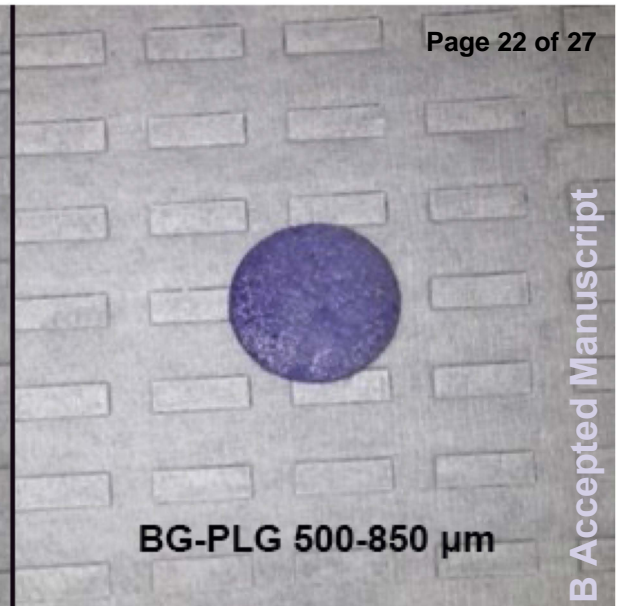
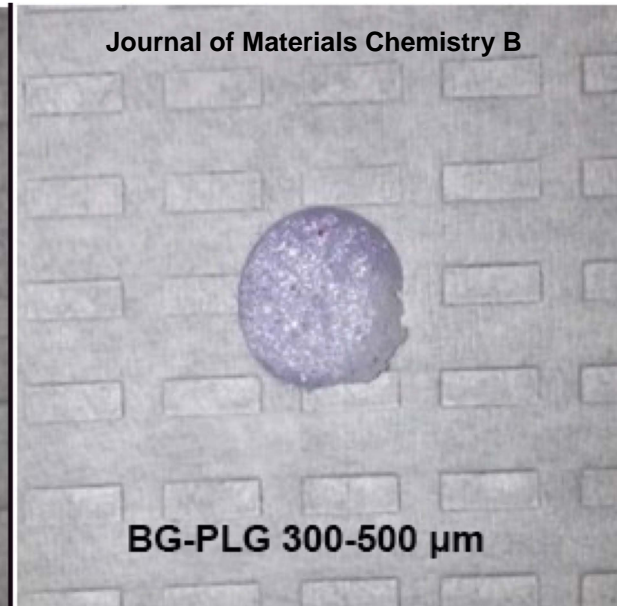
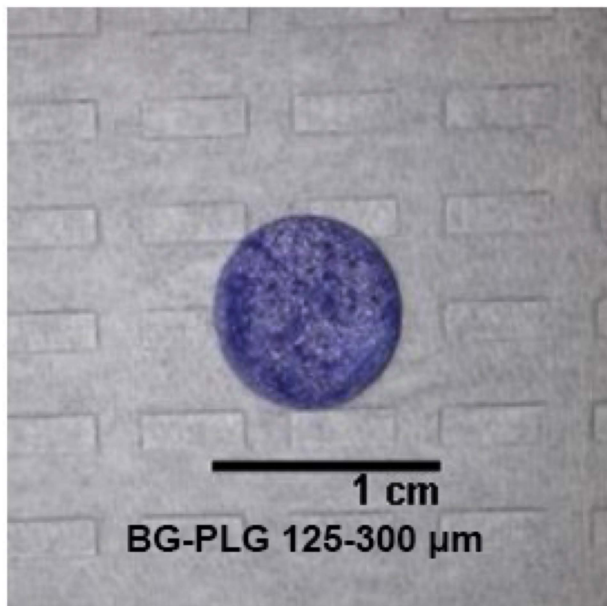
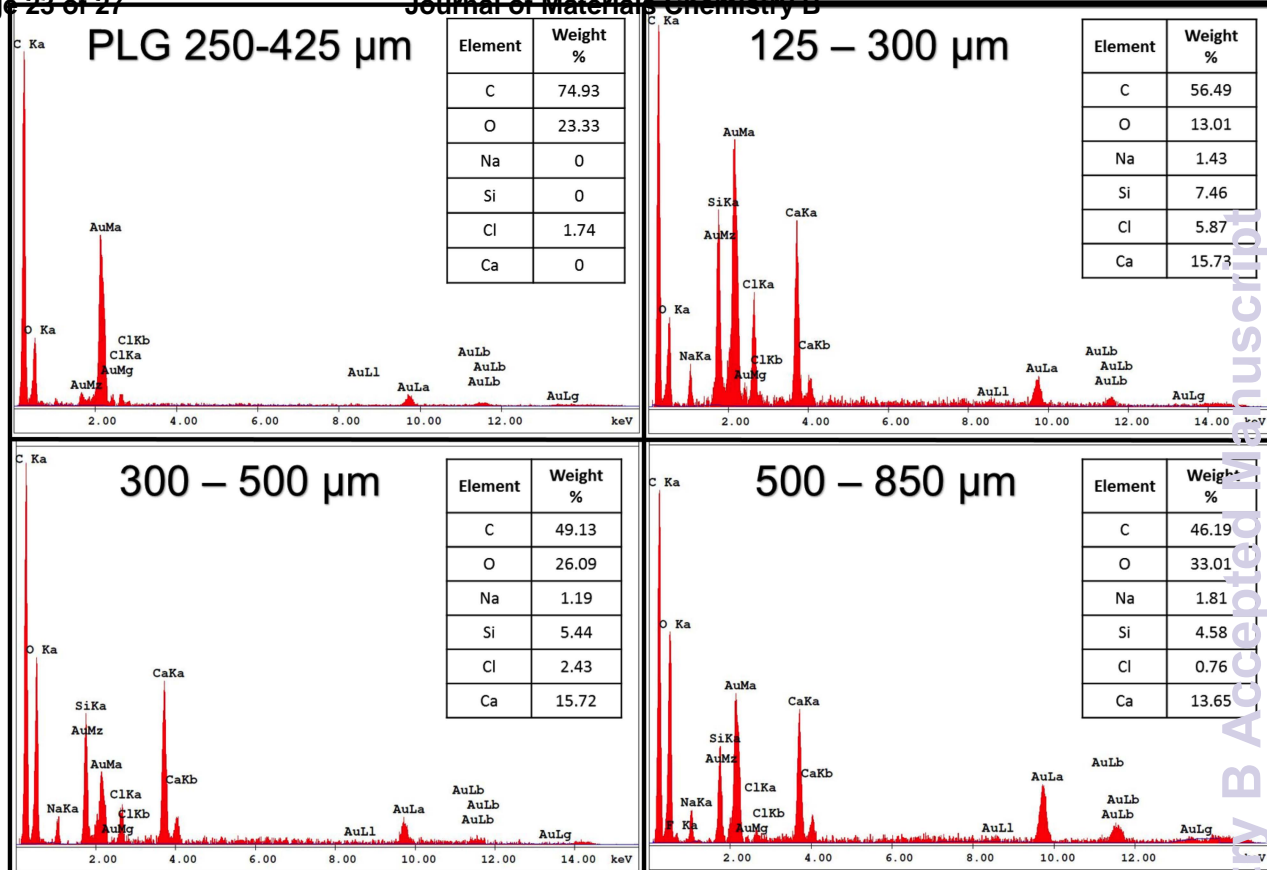


Figure 2



Journal of Materials Chemistry B Accepted Manuscript

Figure 3



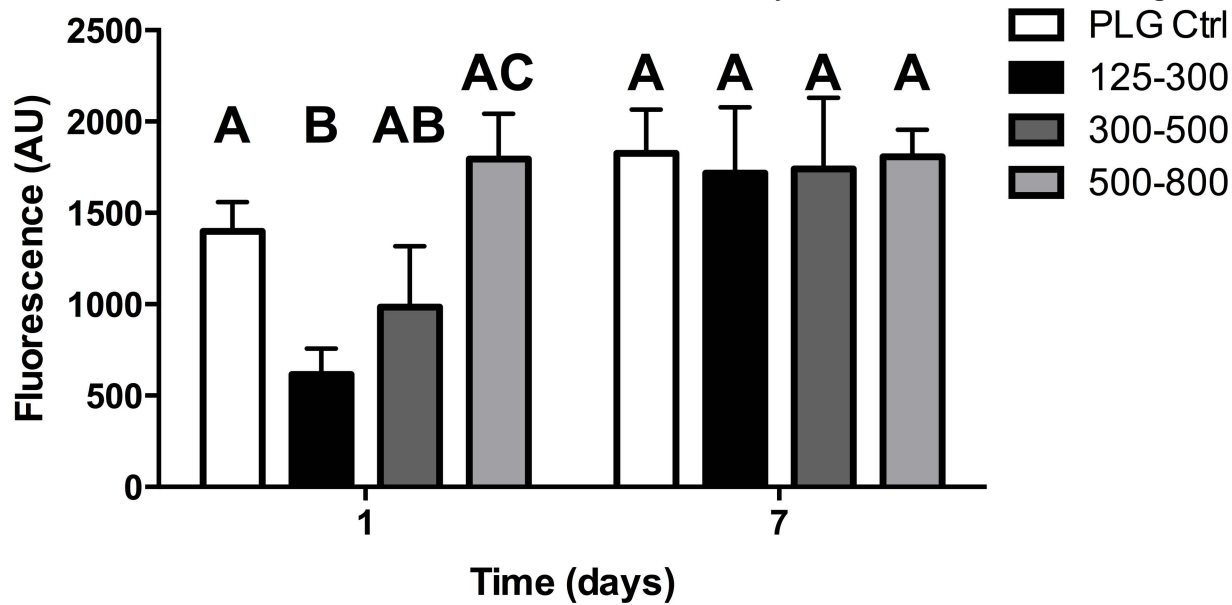
B

Pore size (μm)	%Si \pm STDEV	%Ca \pm STDEV
PLG 250-425	0	0
125-300	0.75 ± 0.29	1.15 ± 0.46
300-500	1.20 ± 0.57	1.52 ± 0.74
500-850	4.20 ± 1.10^a	5.53 ± 1.58^a

C

Pore size (μm)	%Si	%Ca
PLG 250-425	0	0
125-300	-49.1%	+24.8%
300-500	-47.0%	+0.1%
500-850	-53.6%	+350.8%

Figure 4



B

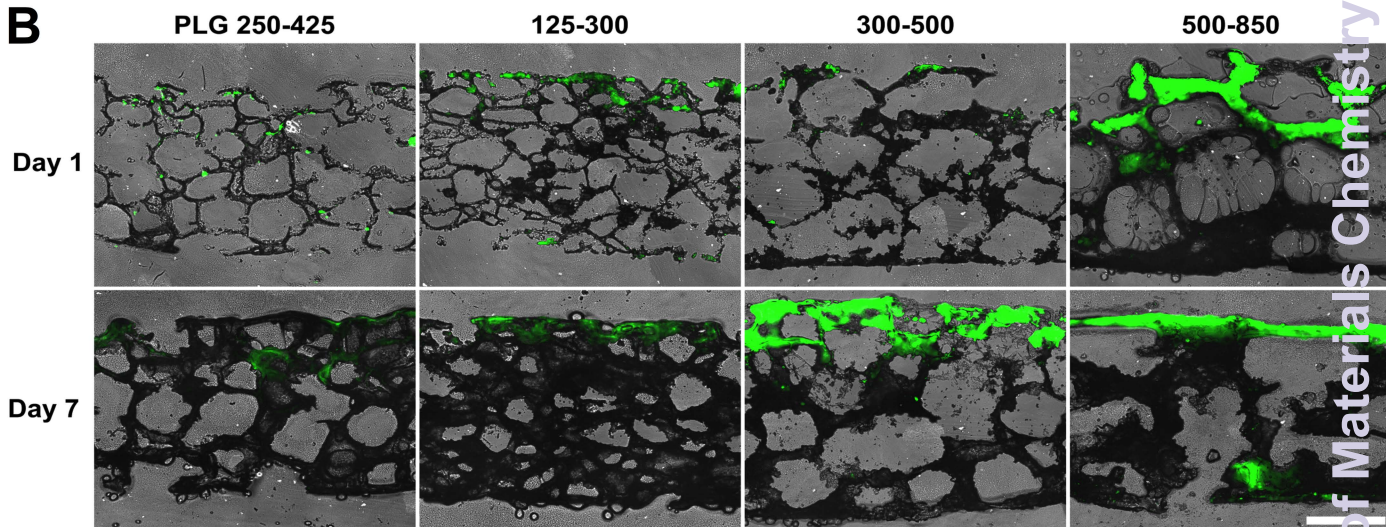
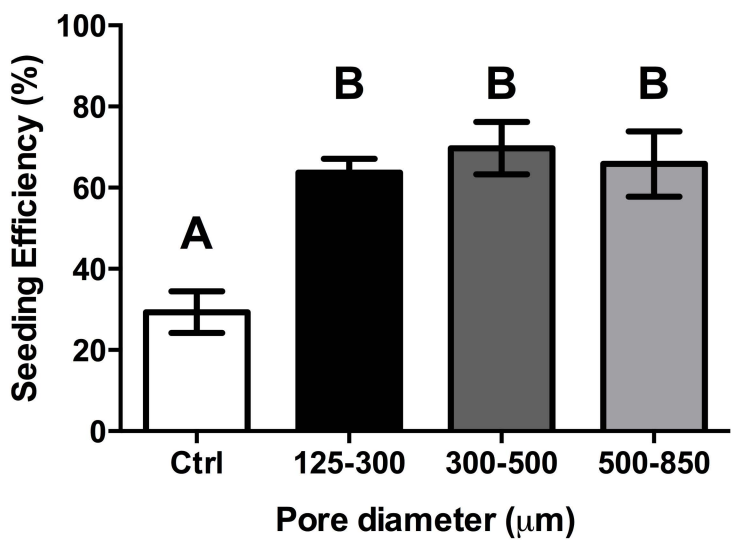
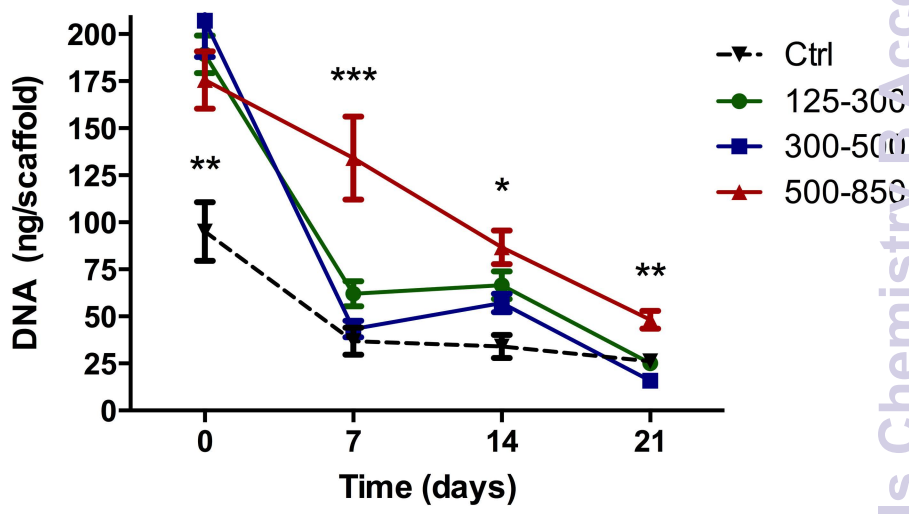


Figure 5

A



B



C

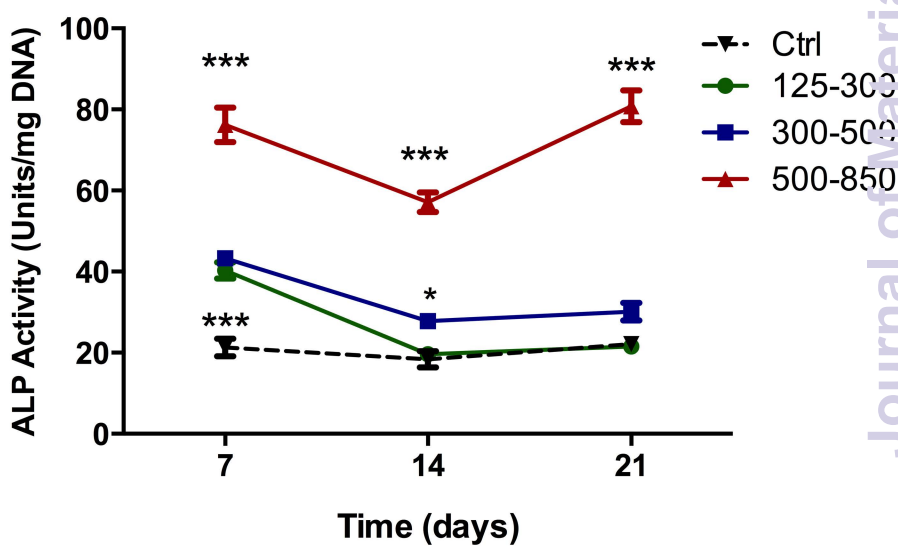
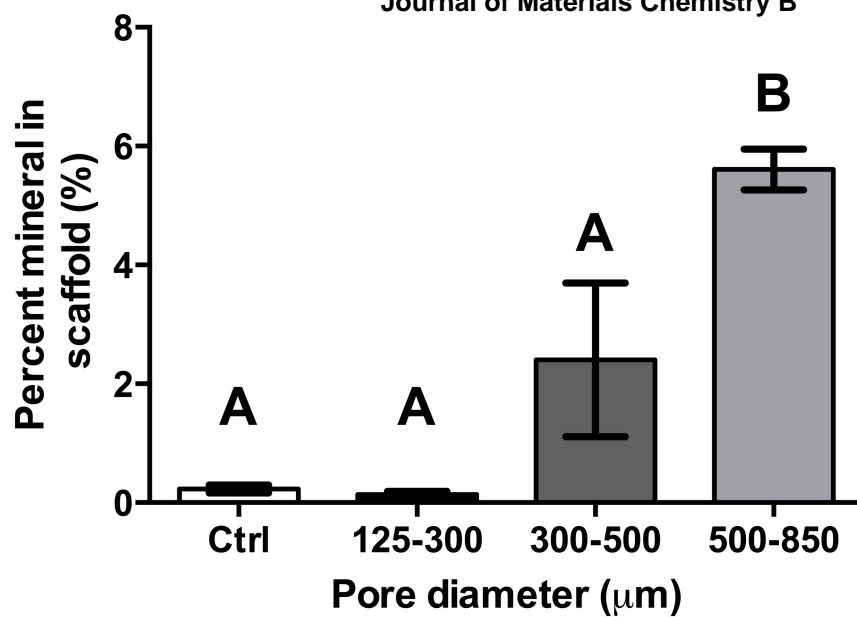
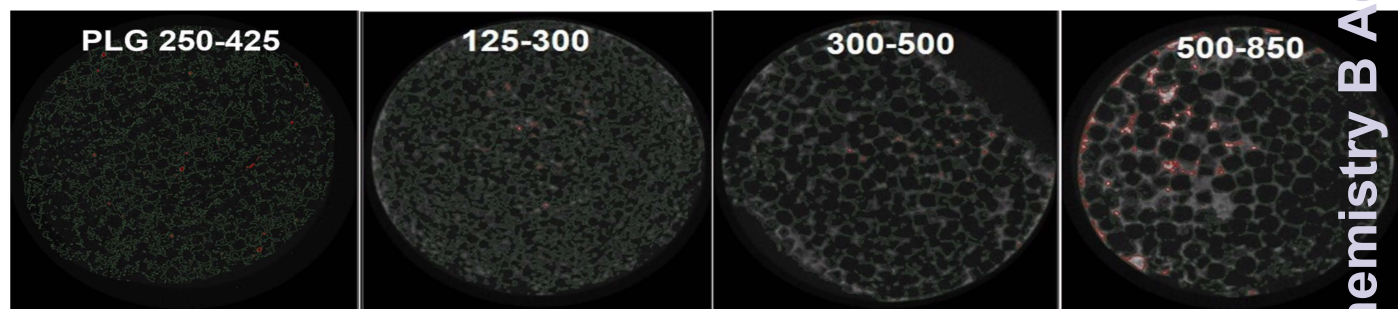
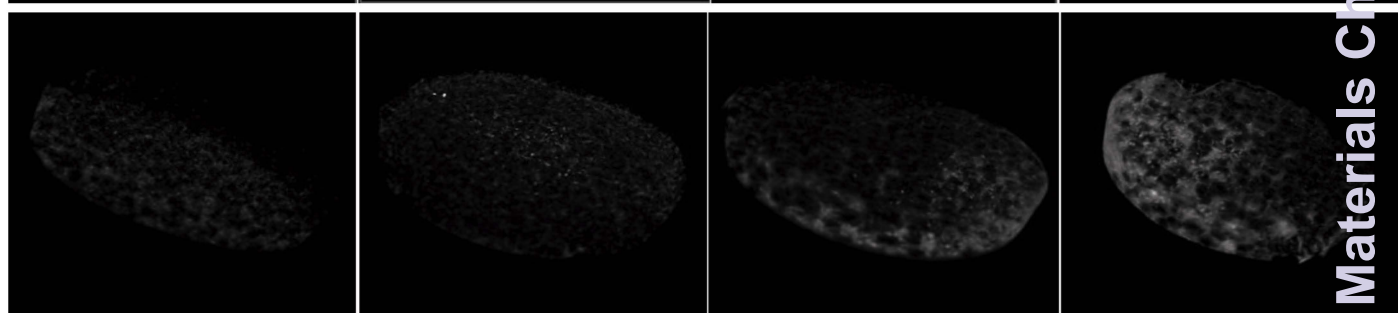


Figure 6

Journal of Materials Chemistry B Accepted Manuscript

A**B****C****Figure 7**

